Progress In Electromagnetics Research Letters, Vol. 51, 39–45, 2015

A Simple Nanoscale Plasmonic Square-Shaped Ring Resonator Waveguide

Ya-Li Yan*, Guang Fu, Yu Zhang, Shu-Xi Gong, and Xi Chen

Abstract—A novel surface plasmon based square-shaped ring resonator with bending metal-dielectric-metal input/output (I/O) waveguide at optical spectral range is investigated. The influence of various geometric parameters is studied in detail, with parallel finite difference time domain method. The results validate that vertical coupling disturbance can be efficiently suppressed by employing the modified I/O structure. The transmittance performance has all the resonant frequencies workable with better extinction ratios, higher finesse and higher Q-factors compared to the original plasmonic micro-ring resonator. From these analyses, it is found that the proposed waveguide is outstanding in aspects of the total field extinction and frequency selectivity characteristic.

1. INTRODUCTION

Plasmonics is a rapidly growing research field [1–3], which covers several aspects of surface plasmons [4, 5] towards realization of surface-plasmon-based devices [6–10]: plasmonic waveguides [11], plasmonic light-emitting devices [12], plasmonic solar cells [13] and plasma-wave THz photodetection [14, 15]. Waveguide-based plasmonic structures utilizing surface plasmon polariton (SPP) are promising for their capability of high subwavelength scale confinement and low propagation loss [16, 17], which could lead to a high-speed, miniaturized and integrated electrooptical technology. Several plasmonic waveguiding structures have been explored, such as metallic nanoparticles [18, 19], metallic strips or nanowires [20, 21], V-grooves [22], and slot waveguides [23].

The waveguides, consisting of metal-dielectric-metal (MDM) structures, have been tremendously studied nowadays, for they allow metals to be structured and characterized on the nanometer scale with strong localization and long propagation length [24–26]. Among these structures, rectangular-shaped ring resonator waveguides present up to two fundamental resonance frequencies and can be applied to make optical range filters with high efficiency and free spectral range [27, 28]. High transmission at the 90° corners [29] in MDM structures makes the rectangular ring oscillators especially attractive for realizing compact plasmonic resonators used as building blocks to support many important nanoscale device functionalities. However, it has been shown that these structures suffer greatly from their exceeding backward propagating interference, which destroys the optical performance of the waveguide. Thus, it is necessary to solve the over-coupling problem in optical region with some structural modifications. Many different ring structures which can reduce the interference have been analyzed [30], such as circular-shaped and racetrack-shaped ring waveguides, but that changes the optical behaviors of the resonators with rectangular-ring cavity. In this paper, for the first time, we embed bends in the input/output (I/O) waveguide to suppress the vertical coupling disturbance and enhance the resonant performance without altering the rectangular ring structure.

The finite difference time domain (FDTD) is one of the most popular numerical techniques for analyzing complex electromagnetic problems [31]. However, the computation in FDTD is time consuming due to the stability criterion condition, referred as Courant-Friedrich-Levy (CFL)

Received 26 November 2014, Accepted 22 December 2014, Scheduled 8 January 2015
* Corresponding author: Ya-Li Yan (astraaea@126.com).
The authors are with the National Key Laboratory of Antenna and Microwave Technology, Xidian University, Xi'an, Shaanxi 710071, China.

condition [32]. Moreover, FDTD demands small spatial meshes for dispersive media, especially in resonant components. One approach to circumventing these problems is to achieve the parallelization of the FDTD method via the realization of the message passing interface (MPI) [33, 34]. In this way, the algorithm can be sped up by utilizing multiple processors on a cluster that performs a single task concurrently, with the processors sharing the computer resources both in terms of memory use and computational effort.

In this paper, a two-dimensional MPI-based FDTD method with perfectly matched layer (PML) absorbing boundary condition is adopted to analyze a new surface plasmon square-ring resonator (SRR) waveguide. We first describe the physical mechanism of the SRR and dispersive-material modeling which we employ to fit the permittivity of metal in near-infrared and visible light ranges. This is followed by solving the optical behaviors of the modified plasmonic micro-ring resonator by properly determining the structural parameters of the I/O waveguide. Finally, the results are compared with those obtained from the conventional SRR. Numerical results demonstrate that the proposed SRR structure can achieve better field extinction, higher finesse and higher quality factor than the conventional one.

2. DEVICE STRUCTURE AND THEORETICAL ANALYSIS

In the following, the dielectric is air with refractive index 1.0, dispersive characteristic of the metallic material is taken into account as silver by the lossy Drude model, which can be expressed as

$$\varepsilon(w) = \varepsilon_\infty - \frac{w_p^2}{w^2 + iw\gamma} = \left(\varepsilon_\infty - \frac{w_p^2}{w^2+\gamma^2}\right) + i\frac{w_p^2\gamma}{w\left(w^2+\gamma^2\right)} \tag{1}$$

where ε_∞ represents the dielectric constant of the material at infinite frequency, ω_p the electron plasma frequency of metals, γ the collision frequency, and ω the incident angular frequency. We choose $\varepsilon_\infty = 3.71$, $\omega_p = 1.38 \times 10^{16}$ Hz and $\gamma = 2.73 \times 10^{13}$ Hz for the Drude modal, which can fit the experimental data well.

The structure of plasmonic square-shaped ring resonator waveguide is plotted in Figure 1(a), which was first presented in [27]. The edge length S of the ring is 725 nm, the distance between the ring structure and the straight I/O MDM waveguide g is 20 nm. The dielectric width d of both the ring and I/O waveguide is chosen as 50 nm, which means only the fundamental transverse magnetic TM_0 waveguide mode exists. The transmission past the resonator in the I/O waveguide is

$$T = \left|\frac{B}{A}\right|^2 = \frac{\alpha^2 + |t|^2 - 2\alpha|t|\cos(\theta+\phi)}{1 + \alpha^2|t|^2 - 2\alpha|t|\cos(\theta+\phi)} \tag{2}$$

where α means the inner circulation factor and is zero without internal loss; $|t|$ is the coupling coefficient; θ and ϕ represent the ring phase shift and the coupler phase shift, respectively. Standing waves can only form within the ring cavity when satisfying the resonant condition $\theta + \phi = 2m\pi$, where m is some integer. When $\alpha = |t|$, the transmission drops to zero due to critical coupling in the outgoing waveguide. The propagation constant β for TM_0 mode can be obtained according to the dispersion relation

$$\tanh\left(\frac{d\sqrt{\beta^2 - k_0^2\varepsilon_d}}{2}\right) = -\frac{\varepsilon_d\sqrt{\beta^2 - k_0^2\varepsilon_m}}{\varepsilon_m\sqrt{\beta^2 - k_0^2\varepsilon_d}} \tag{3}$$

where ε_d and ε_m are, respectively, permittivity of the dielectric and metal. $k_0 = 2\pi/\lambda$ is the wave number of light with wavelength λ in free space. At resonance, the ring cavity meets $4Ln_{eff} = N\lambda_r$, where N is the mode number, λ_r is the resonance wavelength and $n_{eff} = Re[\beta]/k_0$ is the effective index.

Sharp bends of plasmonic SRR waveguide have been shown to be able to support possible high transmittance of waves with low bending losses [29]. However, the disadvantage of the waveguide lies obviously in its perpendicular waveguide coupling. Several structures have been proposed to suppress the coupling interference [30], with altering the optical characteristics of the resonators with rectangular-ring cavity. Here, basing on the primary ring structure, we apply bends before and after the coupling section in the I/O waveguide to avoid the coupling waves to propagate backward and enhance the resonant performance, as shown in Figure 1(b). L_1 is the length of the coupling region, L_2 is the height of the I/O waveguide and other parameters remain the same as their previous values. The structure will be the original SRR waveguide when $L_2 = 0$.

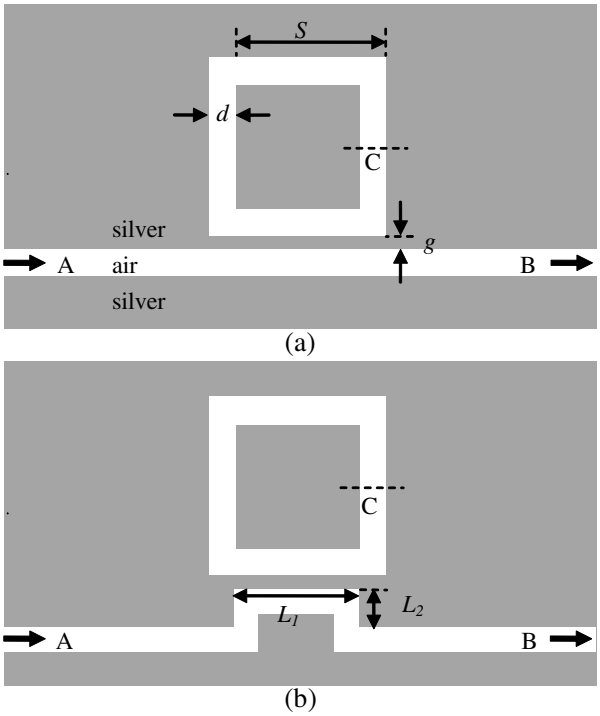

Figure 1. Geometry of SRR with (a) straight I/O waveguide and (b) bending I/O waveguide.

3. NUMERICAL RESULTS

To confirm the above theoretical concept and design principles, the MPI-based FDTD algorithm with PML is utilized to calculate the field propagation characteristic of the proposed SRR structure. In the parallel FDTD simulations, the discretization Cartesian grid sizes are set to be $\Delta x = \Delta y = 1\,\text{nm}$, and the time step is set as $\Delta t = 2 \times 10^{-18}\,\text{s}$. A Gaussian profile excitation with frequency range of 270–600 THz is injected as a source in the input port A, power monitors are set at B and C to detect the transmitted power P_{tra} and the propagated power P_c inside the ring cavity after passing through the coupling region, respectively. The transmission coefficient is defined to be $T = P_{tra}/P_{in}$ and the normalized power is P_c/P_{in}, where P_{in} is the input power of the straight MDM waveguide without the ring resonator.

The spectral responses of the modified SRR for varying L_1 at a fixed height $L_2 = 100\,\text{nm}$, varying L_2 at a fixed length $L_1 = 400\,\text{nm}$ are illustrated in Figure 2. It is observed that the transmission peak value decreases with the increase of the length L_1. This is because that longer L_1 has higher vertical coupling interference so more loss will be generated. The extinction ratio (ER) is used to indicate the power modulation property of the optical resonator. The larger the ER, the easier it will be for the resonator to accurately detect between the on-resonance and off-resonance power levels. The dependence of the ER on the length of L_1 with a given height $L_2 = 100\,\text{nm}$ is shown in Figure 3. As expected, the parallel FDTD algorithm results reveal that the ERs of transmittance at resonant dips of the modified waveguide significantly depend on the choice of the construction of the I/O waveguide. With the increasing of L_1, the ER increases at resonant frequencies around 300 and 440 THz but gets poorer around 370 THz. Figure 2(b) shows that the ER characteristic of these resonances is almost changeless whereas the finesse changes obviously as L_2 alters. On the whole, better field extinction and transmission performance of the modified SRR can be provided when $L_1 = 400\,\text{nm}$ and $L_2 = 100\,\text{nm}$.

Comparison of the normalized power P_c/P_{in} between the original and proposed SRR is depicted in Figure 4. In the proposed SRR, the length L_1 and the height L_2 are, respectively, fixed to be 400 nm and 100 nm. It is obvious that the resonant performance and the energy intensity inside the ring cavity are significantly strengthened by utilizing the bending I/O waveguide, which implies that the field within the ring is more confined and the waves propagating to the input port become less.

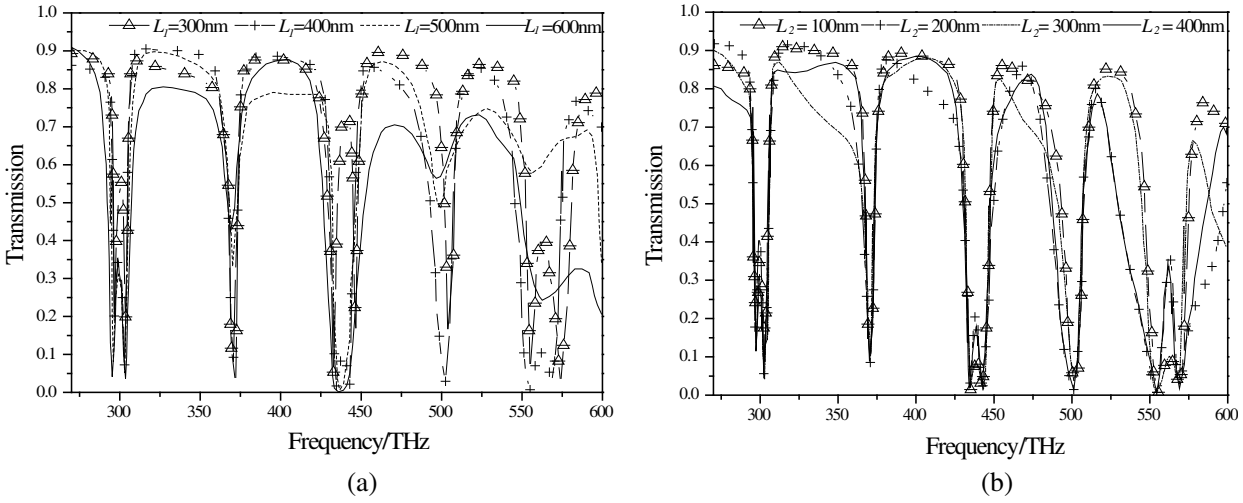

Figure 2. Transmission spectra of the modified SRR with (a) different L_1 at fixed $L_2 = 100\,\text{nm}$ and (b) different heights of L_2 at fixed $L_1 = 400\,\text{nm}$.

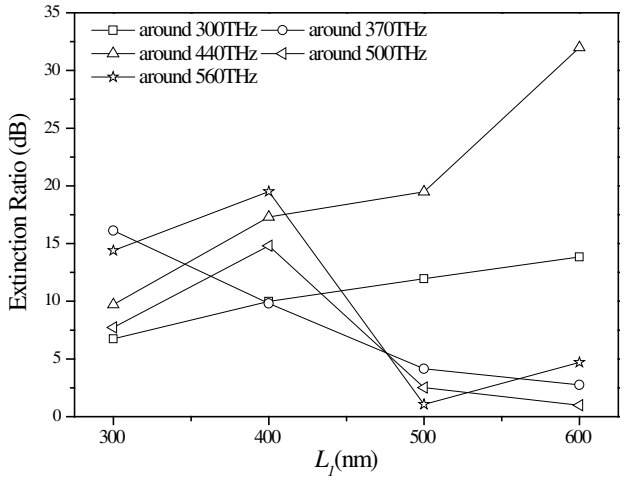

Figure 3. Dependence of extinction ratio on the length of L_1 with $L_2 = 100\,\text{nm}$.

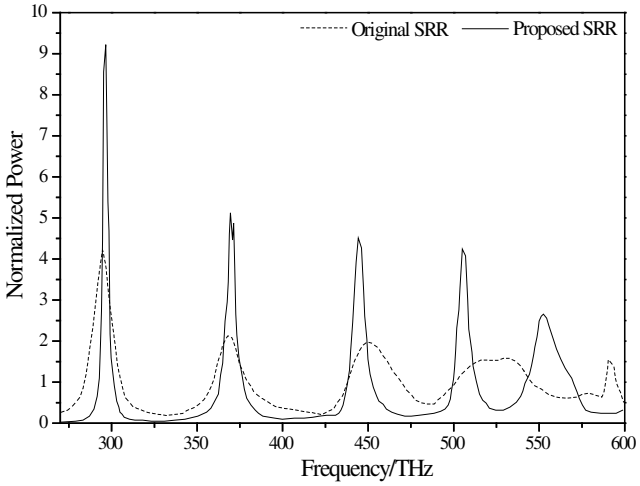

Figure 4. Comparison of the normalized power P_c/P_{in} between the original and proposed SRR.

Figure 5 indicates the comparison of transmission spectra between the original and proposed SRR. For mode number $N = 4$, the resonant wavelength is expected to be at $\lambda_r = 1005\,\text{nm}$ ($n_{eff} = 1.3873$), while the calculated spectra exhibits two resonances at 989 nm and 1008 nm. The reason is that the resonant modes is divided into two standing-wave resonance modes owing to the nonuniform distribution of effective index surround the SRR [27]. It shows that the transmittance response for the constructed SRR has all the resonant dips less than 10% at frequencies 297.6, 303.4, 371.3, 435.3, 443, 502.5, 555.3 and 569.1 THz, but in the case of original SRR only the frequencies around 300 THz are workable. At the same time, the minimum ER value largely increases from 1.18 dB to 9.82 dB, which makes the SRR more competitive with other resonators. The quality factor $Q = f_c/FWHM$ (where f_c is the central frequency and $FWHM$ is the full width at half maximum) is a critical characteristic of a resonator, which describes the lifetime of the resonance. One can find that the $FWHM$ becomes finer in the modified SRR, so higher Q-factors can be achieved. For example, $Q = 67.44$ can be obtained when $f_c = 370.9\,\text{THz}$, which is comparable to the original SRR configuration $Q = 25.43$ (when $f_c = 368.8\,\text{THz}$). Higher Q-factor infers the field oscillation along the ring resonator will die out more slowly. Furthermore, larger maximum transmission amplitude at resonance can be gained in the proposed waveguide. Consequently,

the plamonic SRR with bends embedded into the bottom MDM waveguide can perform better in optical behaviors compared with the conventional one.

The magnetic field H_z distributions corresponding to eight resonances are shown in Figures 6(a)–(h). The standing waves building up within the ring have their peak values at the corners in Figure 6(a), and the resonance concentrates at the edges of the square in Figure 6(b). In both cases, the cavity mode number N is 4. One can find that as the resonant frequency increases, the difference of the field intensity between the edge and the corner decreases, because more wave cycles are generated to fit the ring structure. The field distributes symmetrically or anti-symmetrically at different resonant frequencies. In the original SRR, the incident waves at the input port will be seriously enhanced by the constructive interference. In Figure 6, it is observed that no waves propagate to the output port, and just few waves at the left of the bottom waveguide are enhanced. This means when waves propagate along the

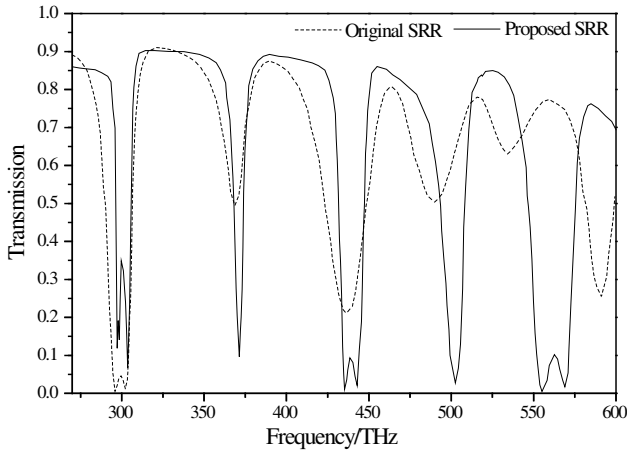

Figure 5. Comparison of transmission spectra between the original and proposed SRR.

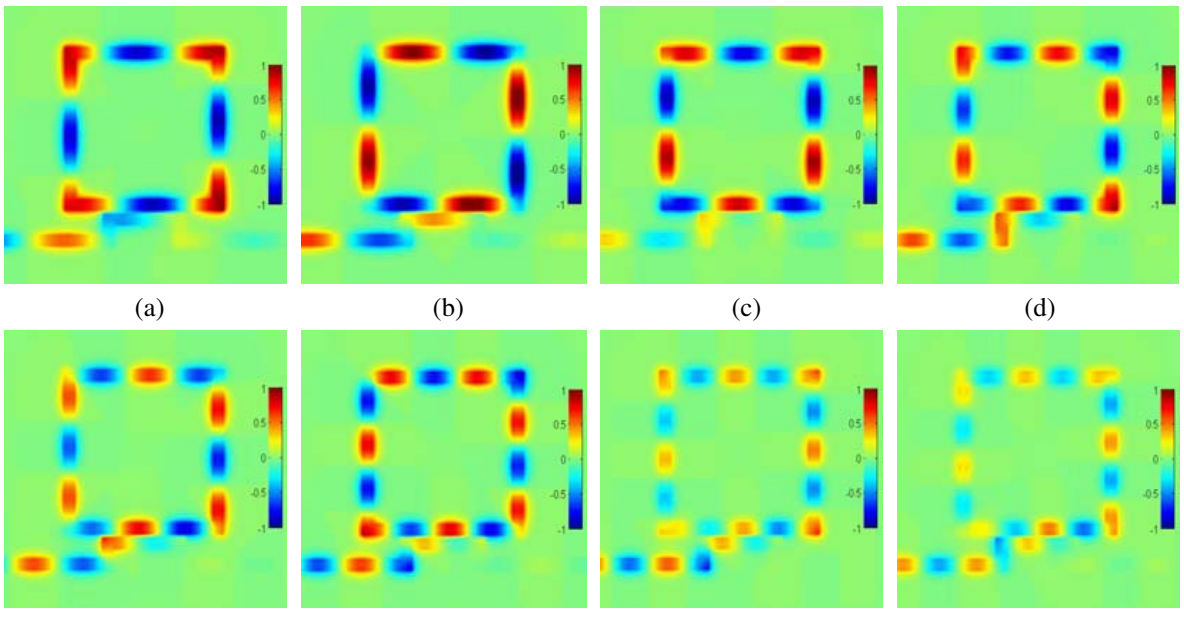

Figure 6. Parallel FDTD simulation results for the proposed square-shaped ring resonator, showing the *Hz* distributions at each resonant dip at (a) 297.6 THz, (b) 303.4 THz, (c) 371.3 THz, (d) 435.3 THz, (e) 443 THz, (f) 502.5 THz, (g) 555.3 THz and (h) 569.1 THz.

last vertical corner of the ring cavity, the modified bending coupling region effectively suppresses the coupling waves to go backward.

4. CONCLUSION

We elucidate a novel plasmonic square-shaped ring resonator coupled with bending input/output MDM waveguide in this paper. The parallel MPI-based FDTD algorithm demonstrates that vertical coupling interference can be significantly suppressed in the constructed structure, which solves the radiated problem of surface plasmon based ring resonators. The transmittance response has all the resonances workable with better extinction ratios, higher finesse and higher Q-factors, when compared with the results obtained from the conventional SRR. It makes these micro-ring resonator structures more functional and promising for integrated optical circuit applications.

ACKNOWLEDGMENT

This work is supported by the National High Technology Research and Development Program of China (863 Program) (2012AA01A308), the NSFC (61301069, 61072019), the Program for New Century Excellent Talents in University of China (NCET-13-0949) and the project with contract No. 2013KJXX-67, The computational resources utilized in this research are provided by Shanghai Supercomputer Center.

REFERENCES

1. Tassin, P., T. Koschny, M. Kafesaki, and C. M. Soukoulis, "A comparison of graphene, superconductors and metals as conductors for metamaterials and plasmonics," *Nature Photonics*, Vol. 6, No. 4, 259–264, 2012.
2. Kauranen, M. and A. V. Zayats, "Nonlinear plasmonics," *Nature Photonics*, Vol. 6, 737–748, 2012.
3. Politano, A., "Interplay of structural and temperature effects on plasmonic excitations at noble-metal interfaces," *Philosophical Magazine*, Vol. 92, No. 6, 768–778, 2012.
4. Politano, A., A. R. Marino, V. Formoso, D. Farias, R. Miranda, and G. Chiarello, "Quadratic dispersion and damping processes of π plasmon in monolayer graphene on Pt(111)," *Plasmonics*, Vol. 7, No. 2, 369–376, 2012.
5. Politano, A., V. Formoso, and G. Chiarello, "Collective electronic excitations in thin Ag films on Ni(111)," *Plasmonics*, Vol. 8, No. 4, 1683–1690, 2013.
6. Politano, A. and G. Chiarello, "Unravelling suitable graphene-metal contacts for graphene-based plasmonic devices," *Nanoscale*, Vol. 5, No. 17, 8215–8220, 2013.
7. Politano, A. and G. Chiarello, "Quenching of plasmons modes in air-exposed graphene-Ru contacts for plasmonic devices," *Applied Physics Letters*, Vol. 102, No. 20, 201608, 2013.
8. Yan, H. G., X. S. Li, B. Chandra, G. Tulevski, Y. Q. Wu, M. Freitag, W. J. Zhu, P. Avouris, and F. N. Xia, "Tunable infrared plasmonic devices using graphene/insulator stacks," *Nature Nanotechnology*, Vol. 7, No. 5, 330, 2012.
9. Zheludev, N. I., "Photonic-plasmonic devices: A 7-nm light pen makes its mark," *Nature Nanotechnology*, Vol. 5, No. 1, 10–11, 2010.
10. Politano, A., "Influence of structural and electronic properties on the collective excitations of Ag/Cu(111)," *Plasmonics*, Vol. 7, No. 1, 131–136, 2012.
11. He, X. Y., Q. J. Wang, and S. F. Yu, "Numerical study of gain-assisted terahertz hybrid plasmonic waveguide," *Plasmonics*, Vol. 7, No. 3, 571–577, 2012.
12. Okamoto, K., I. Niki, A. Shvartser, Y. Narukawa, T. Mukai, and A. Scherer, "Surface-plasmon-enhanced light emitters based on InGaN quantum wells," *Nature Material*, Vol. 3, No. 9, 601–605, 2004.
13. Reineck, P., G. P. Lee, D. Brick, M. Karg, P. Mulvaney, and U. Bach, "A solid-state plasmonic solar cell via metal nanoparticle self-assembly," *Advanced Materials*, Vol. 24, No. 35, 2012.

14. Yao, X. H., M. Tokman, and A. Belyanin, "Efficient nonlinear generation of THz plasmons in graphene and topological insulators," *Physical Review Letters*, Vol. 112, No. 5, 055501, 2014.
15. Lu, L., B. Geng, J. Horng, C. Girit, M. Martin, Z. Hao, H. A. Bechel, X. G. Liang, A. Zettl, Y. R. Shen, and F. Wang, "Graphene plasmonics for tunable terahertz metamaterials," *Nature Nanotechnology*, Vol. 6, 630–634, 2011.
16. Takahara, J., S. Yamagishi, H. Taki, A. Morimoto, and T. Kobayashi, "Guiding of a one-dimensional optical beam with nanometer diameter," *Optics Letters*, Vol. 22, 475–477, 1997.
17. Djabery, R., S. Nikmehr, and S. Hosseinzadeh, "Grating effects on sidelobe suppression in MIM plasmonic filters," *Progress In Electromagnetics Research*, Vol. 135, 271–280, 2013.
18. Liaw, J. W., M. K. Kuo, and C. N. Liao, "Plasmon resonances of spherical and ellipsoidal nanoparticles," *Journal of Electromagnetic Waves and Applications*, Vol. 19, No. 13, 1787–1794, 2005.
19. Lee, K. H., I. Ahmed, R. S. M. Goh, E. H. Khoo, E. P. Li, and T. G. G. Hung, "Implementation of the FDTD method based on Lorentz-Drude dispersive model on GPU for plasmonic applications," *Progress In Electromagnetics Research*, Vol. 116, 441–456, 2011.
20. Berini, P., "Plasmon-polariton waves guided by thin lossy metal films of finite width: Bound modes of symmetric structures," *Physical Review B*, Vol. 61, No. 15, 10484–10503, 2000.
21. Weeber, J. C., A. Dereux, C. Girard, J. R. Krenn, and J. P. Goudonnet, "Plasmon polaritons of metallic nanowires for controlling submicron propagation of light," *Physical Review B*, Vol. 60, No. 12, 9061–9068, 1999.
22. Bozhevolnyi, S. I., V. S. Volkov, E. Devaux, J. Y. Laluet, and T. W. Ebbesen, "Channel plasmon subwavelength waveguide components including interferometers and ring resonators," *Nature*, Vol. 440, 508–511, 2006.
23. Veronis, G. and S. Fan, "Modes of subwavelength plasmonic slot waveguides," *Journal of Lightwave Technology*, Vol. 25, No. 9, 2511–2521, 2007.
24. Barnes, W. L., A. Dereux, and T. W. Ebbesen, "Surface plasmon subwavelength optics," *Nature*, Vol. 424, 824–830, 2003.
25. Xu, Y., J. Zhang, and G. F. Song, "Slow surface plasmons in plasmonic grating waveguide," *IEEE Photonics Technology Letters*, Vol. 25, No. 5, 410–413, Jan. 2013.
26. Song, Y., J. Wang, M. Yan, and M. Qiu, "Efficient coupling between dielectric and hybrid plasmonic waveguides by multimode interference power splitter," *Journal of Optics*, Vol. 13, 2011.
27. Hosseini, A. and Y. Massoud, "Nanoscale surface plasmon based resonator using rectangular geometry," *Applied Physics Letters*, Vol. 90, 181102, 2007.
28. Liu, J. L., G. Y. Fang, H. F. Zhao, Y. Zhang, and S. T. Liu, "Plasmon flow control at gap waveguide junctions using square ring resonators," *Journal of Physics D: Applied Physics*, Vol. 43, 055103, 2010.
29. Veronis, G. and S. Fan, "Bends and splitters in metal-dielectric-metal subwavelength plasmonic waveguides," *Applied Physics Letters*, Vol. 83, 131102, 2005.
30. Chung, S. Y., C. Y. Wang, C. H. Teng, C. P. Chen, and H. C. Chang, "Simulations of dielectric and plasmonic waveguide-coupled ring resonators using the legendre pseudospectral time-domain method," *Journal of Lightwave Technology*, Vol. 30, No. 11, 1733–1742, 2012.
31. Taflove, A. and S. C. Hagness, *Computational Electrodynamics: The Finite Difference Time Domain Method*, 3rd Edition, Artech House, Norwood, MA, 2005.
32. Lakshmikanthan, V. and D. Trigiante, *Theory of Difference Equations: Numerical Methods and Applications*, Academic, 1988.
33. Guiaut, C. and K. Mahdjoubi, "A parallel FDTD algorithm using the MPI library," *IEEE Antennas and Propagation Magazine*, Vol. 43, 94–103, 2001.
34. Yu, W., R. Mittra, T. Su, Y. J. Liu, and X. L. Yang, *Parallel Finite-difference Time-domain Method*, Artech House, 2006.